FARADAY

Photoacoustic study on the structural transformation of $AlPO_4$-21/$AlPO_4$-25 and $AlPO_4$–H_3/$AlPO_4$–C/$AlPO_4$–D

Man-Hyoung Ryoo and Hakze Chon*

Department of Chemistry, Korea Advanced Institute of Science and Technology, Taeduck Science Town, Taejon 305-701, Korea

A temperature-dependent photoacoustic technique was used to elucidate the structural transformation of aluminophosphate molecular sieves, $AlPO_4$-21/$AlPO_4$-25 and $AlPO_4$–H_3/$AlPO_4$–C/$AlPO_5$–D. The definite transformation temperature of $AlPO_4$-21 into $AlPO_4$-25 was obtained at *ca.* 537 K. In a parallel photoacoustic study on the structural transformation of $AlPO_4$–H_3/$AlPO_4$–C/$AlPO_4$–D, the photoacoustic results suggest that the structural transition of $AlPO_4$–H_3 into $AlPO_4$–C occurs at *ca.* 378 K, and the topotactic transformation of $AlPO_4$–C into $AlPO_4$–D takes place at *ca.* 497 K.

Introduction

The photoacoustic effect (PAE) has been used to investigate phase transitions in solid materials.[1–6] The application of a temperature-dependent PA technique to the structural transformation of zeolite molecular sieves has special merit. The desorption of water molecules in zeolite materials during heating results in a strong increase in the background PA signal. The increase in the PA signal helps to define the structural transition of zeolite materials more clearly. In a conventional calorimetric method, however, these two endothermic processes, dehydration and structural transition, cannot be distinguished.

In the present study, the transition temperature of the structural transformation of $AlPO_4$-21 into $AlPO_4$-25 is defined using a temperature-dependent PA technique. A parallel PA experiment on $AlPO_4$–H_3 undergoing a similar structural transition into $AlPO_4$–C and subsequent transition into $AlPO_4$–D upon heating is also performed.

Experimental

The aluminophosphate molecular sieves $AlPO_4$-21 and $AlPO_4$–H_3 were synthesized from the following gel mixtures: $AlPO_4$-21—1 Al_2O_3 : 1 P_2O_5 : 1 *n*-propylamine : 20 H_2O at 458 K for 40 h; $AlPO_4$–H_3—1 Al_2O_3 : 1 P_2O_5 : 1 di-*n*-propylamine : 40 H_2O at 418 K for 20 h.

Pseudoboehmite (74.2% Al_2O_5, Capatal-B from Vista) and phosphoric acid (85 mass%, from Junsei) were used as sources of aluminium and phosphorus. The *n*-propylamine and di-*n*-propylamine were used as template agents (from Aldrich). The $AlPO_4$-25 sample was obtained by calcining $AlPO_4$-21 at 773 K for 24 h.

The home-built PA measuring system has been described previously.[7] A 10 mW He–Ne laser was used as a light source. The PA cell body was made of a stainless-steel block. For sealing acoustic waves in the cell, a quartz window and aluminium foil spacer were used. The PA spectra were obtained by continuously changing the temperature at a rate of 1 K min^{-1}.

The output of the PA signal was detected by an electret microphone connected to the PA cell body through a waveguide tube, giving the form of a Helmholtz resonator. PA measurements were carried out using a mechanical chopper (EG & G PARC 125 A) at a chopping frequency of 25 Hz. The temperature of a sample was measured with a thermocouple placed in close contact with the sample compartment through a small hole in the cell body. The PA signal was analysed using a lock-in amplifier (SRS 510). The PA measurements on $AlPO_4$–H_3 were carried out using the sample mixed with Carbon Black to enhance the PA signal.

Thermal analysis [thermogravimetry (TG) and differential thermal analysis (DTA)] was performed with a Setaram TG 92-12 at a heating rate of 1 K min^{-1} under a flow of air. X-Ray diffraction (XRD) patterns were obtained using a Rigaku model D/MAX-RB which had a high temperature measurement attachment with Cu-Kα radiation at a heating rate of 1 K min^{-1}.

Results and Discussion

The X-ray powder diffraction patterns of the as-synthesized $AlPO_4$-21 and $AlPO_4$–H_3 were in good agreement with those in the literature.[8,9]

The thermal analysis curves of as-synthesized $AlPO_4$-21 are given in Fig. 1. One-step mass loss of around 16.8% was observed in the 503–593 K temperature region. A weak and broad endothermic peak was observed at *ca.* 540 K due to the desorption of water molecules, while a strong exothermic peak from the oxidation of organic templates was observed at *ca.* 573 K.

Temperature-dependent PA spectra of $AlPO_4$-21 and $AlPO_4$-25 are given in Fig. 2. In the PA spectra of $AlPO_4$-21 a sharp decrease in the PA signal intensity is observed at *ca.* 537 K during an increase in the PA signal. The PA spectra of the $AlPO_4$-25 samples, however, show only a strong band, having a maxima at *ca.* 393 K, on heating.

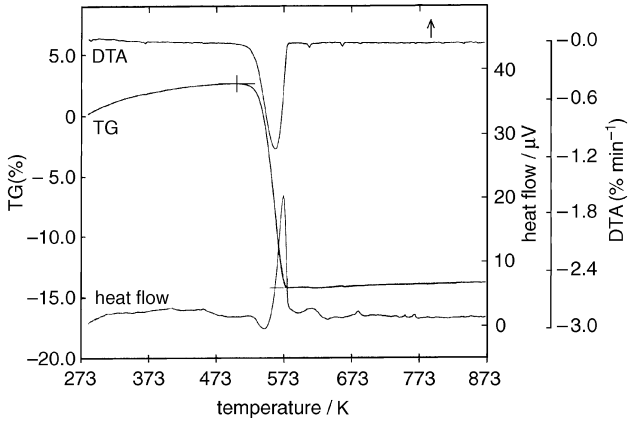

Fig. 1 DTA and TG curves for $AlPO_4$-21

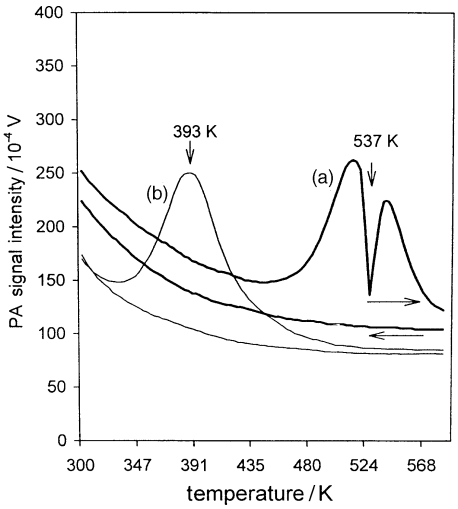

Fig. 2 Temperature dependence of the PA signal of (a) $AlPO_4$-21 (bold lines) and (b) $AlPO_4$-25 samples (→, temperature increasing; and ←, temperature decreasing)

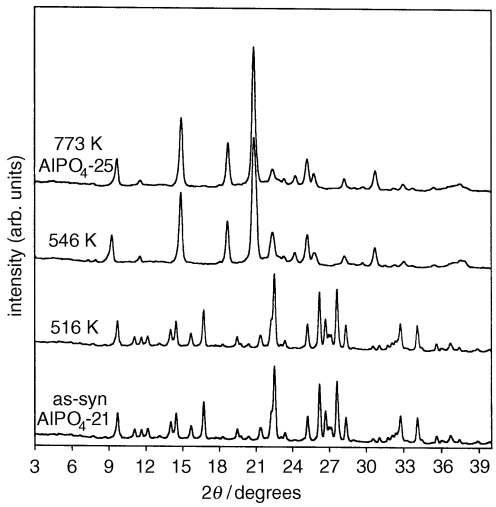

Fig. 3 XRD patterns observed during heating of as-synthesized $AlPO_4$-21 samples at a heating rate of 1 K min^{-1}. The typical XRD patterns for $AlPO_4$-21 and $AlPO_4$-25 were observed at *ca.* 516 K and 546 K, respectively.

The increase in the PA signal intensity is attributed to the desorption of water molecules from the channels of the zeolite molecular sieves. The desorbing water vapour can cause a momentary increase in pressure within the PA cell, resulting in an enhancement of the PA signal intensity. The enhancement of the PA signal from solid materials due to the presence of liquid vapours has been called the 'adsorbed piston effect' by Ganguly and Somasundaram.[10,11]

It is worth noticing that there is a strong increase in PA signal due to the dehydration of water molecules from the channels of the zeolite material, though this process is endothermic. In thermally thick and optically opaque samples, the PA signal decreases slowly as the temperature rises.[12]

The sharp PA decrease at *ca.* 537 K observed in the PA spectra of $AlPO_4$-21 samples suggests that a process other than dehydration occurred upon heating. The process can be assigned to the structural transformation of $AlPO_4$-21 into $AlPO_4$-25 by the removal of bridging hydroxy groups in the $AlPO_4$-21 lattice.

In the as-synthesized $AlPO_4$-21 structure proposed elsewhere,[13–17] the phosphorus atoms are in tetrahedral (IV) coordination while the aluminium atoms are split one-third into tetrahedral (IV) and two-thirds into trigonal-bipyramidal (V) coordination. The two five-coordinated aluminium atoms and the one four-coordinated phosphorus atom form unique three-membered rings with a bridging hydroxy group between the two aluminium atoms. It has been reported that the bridging hydroxy groups are removed upon heating, leading to the structural transformation into $AlPO_4$-25.[13–17] The endothermic breakage of the bonds between the aluminium and the oxygen of the bridging hydroxy groups, which occurs during the structural transformation, acts as a heat sink for the available heat in the sample and the gas phase within the PA cell. This results in a sharp decrease of the PA signal at *ca.* 537 K.

The typical XRD patterns for $AlPO_4$-21 and $AlPO_4$-25 were obtained at *ca.* 516 and 546 K, respectively. This result, *i.e.* the observation of different crystalline phases before and after the PA signal decrease, suggests that the sharp decrease in the PA signal intensity can be attributed to the structural transition process. The XRD patterns are given in Fig. 3.

In the $AlPO_4$-21 and $AlPO_4$-25 samples, the dehydration process causing the enhanced PA signal takes place over different temperature ranges. This can probably be attributed to the different structural constraints in these samples. The shape of the $AlPO_4$-21 channels is significantly distorted compared with that of $AlPO_4$-25, by the presence of the bridging hydroxy groups.[13,14] In practice, the dehydration process is highly dependent on both the shape and the size of the channels within the molecular sieves. The dehydration of aluminophosphate materials, such as $AlPO_4$-11, $AlPO_4$-5 and $AlPO_4$-8, occurs at *ca.* 533, 440 and 430 K, respectively. $AlPO_4$-11 has a 10-membered elliptical channel structure, whereas $AlPO_4$-5 and $AlPO_4$-8 have 12- and 14-membered straight channel structures, respectively.[18]

The organic template *n*-propylamine, encapsulated during the synthesis of $AlPO_4$-21, seems to have no effect on the variations of PA signal intensity caused by the structural transformation and dehydration processes. The organic template was removed at *ca.* 573 K after a complete structural transition into $AlPO_4$-25, as shown in the thermal analysis (Fig. 1).

Parallel PA experiments on the $AlPO_4$–H_3 samples were performed upon heating. It has been reported that the $AlPO_4$–H_3 framework, having PO_4 alternating with AlO_4 tetrahedra and $AlO_4(H_2O)_2$ octahedra, transforms into $AlPO_4$–C by removal of the two coordinated water molecules from the octahedral aluminium, and that the AlO_4–C subsequently transforms into $AlPO_4$–D by a rearrangement of the bonding sequence.[8,19,20]

In Fig. 4, a temperature-dependent PA observation of the

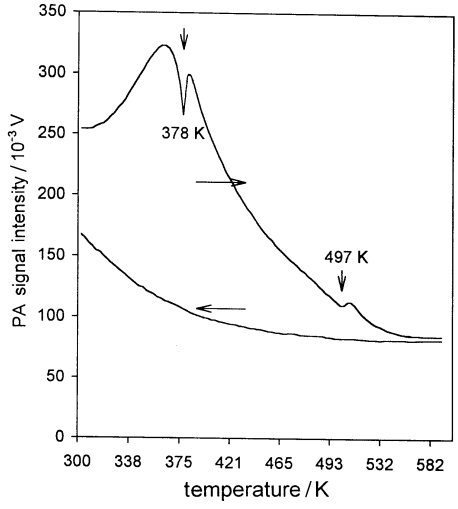

Fig. 4 Temperature dependence of the PA signal of $AlPO_4$–H_3 sample (→, temperature increasing; and ←, temperature decreasing)

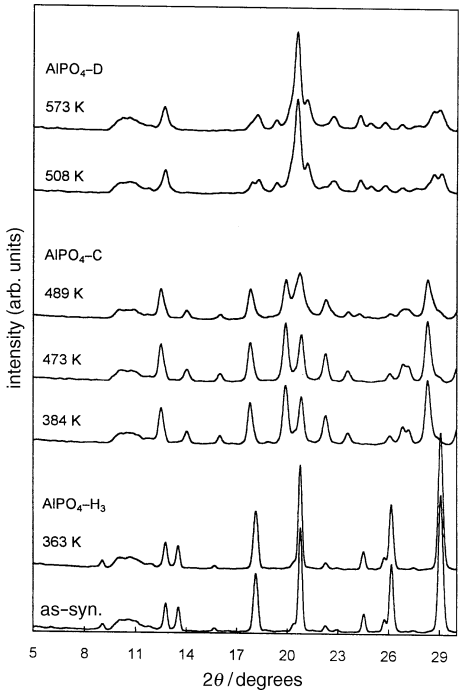

Fig. 5 XRD patterns observed during heating of the as-synthesized $AlPO_4$–H_3 sample at a heating rate of 1 K min^{-1}. The typical XRD patterns for $AlPO_4$–H_3, $AlPO_4$–C and $AlPO_4$–D were observed in the temperature ranges between the two PA signal drops. (The broad bands at *ca.* $2\theta \approx 10°$ are caused by the diffraction of the sample holder.)

$AlPO_4$–H_3 sample shows the two decreases in PA signal. One is observed at *ca.* 378 K during a strong increase of background PA signal, due to the dehydration process; the other is observed at *ca.* 497 K. The decrease in PA signal intensity at *ca.* 497 K is much less pronounced than that at *ca.* 378 K and is attributed to the different amount of dehydration in the zeolite sample around this temperature region as the PA signal decreases.

The two decreases in PA signal are attributed to the structural transformation processes. In XRD experiments on the $AlPO_4$–H_3 samples during heating, the typical XRD patterns for $AlPO_4$–H_3 and $AlPO_4$–C were obtained before and after the PA signal decrease at *ca.* 378 K, which is similar to results obtained in XRD measurement of $AlPO_4$-21. Those for $AlPO_4$–D were observed after the second PA decrease at *ca.* 497 K (Fig. 5).

The sharp decrease at *ca.* 378 K can be assigned to the structural transformation of $AlPO_4$–H_3 into $AlPO_4$–C by an endothermic removal of two coordinated water molecules of octahedral aluminium from the $AlPO_4$–H_3 lattice[8,19,20] and that at *ca.* 497 K to a bond breakage during the topotactic phase transformation of $AlPO_4$–C into $AlPO_4$–D.[8,20] The temperatures for the structural transformations of $AlPO_4$–H_3 → $AlPO_4$–C and $AlPO_4$–C → $AlPO_4$–D were found at *ca.* 378 and 497 K, respectively.

Conclusion

The definite temperature for structural transition of $AlPO_4$-21 into $AlPO_4$-25 was at *ca.* 537 K. The transformation temperatures of $AlPO_4$–H_3 into $AlPO_4$–C and subsequent transition into $AlPO_4$–D were at *ca.* 378 and 497 K, respectively. The PA signal decrease due to the endothermic structural transformation taking place in zeolite molecular sieves is made more pronounced by the presence of a dehydration process. The results suggest that a PA method can be a useful tool to study the structural transition of zeolite materials.

References

1 R. Florin, J. Pelzl, M. Rosenberg, H. Vargas and R. Wernhardt, *Phys. Status Solidi A*, 1978, **48**, K35.
2 C. Pichon, M. L. Liboux, D. Fournier and A. C. Boccara, *Appl. Phys. Lett.*, 1979, **35**, 435.
3 M. A. A. Siqueira, C. C. Ghizoni, J. L. Vargas, E. A. Menezes, H. Vagas and L. C. Miranda, *J. Appl. Phys.*, 1980, **51**, 1403.
4 P. Korpium and R. Tilgner, *J. Appl. Phys.*, 1980, **51**, 6115.
5 P. Korpium, J. Baumann, E. Lüscher, E. Papamokos and R. Tilgner, *Phys. Status Solidi A*, 1980, **58**, K13.
6 P. S. Bechthold, M. Campagna and T. Schober, *Solid State Commun.*, 1980, **36**, 225.
7 K-Y. Lee and H. Chon, *J. Catal.*, 1990, **126**, 677.
8 R. Szostak, *Handbook of Molecular Sieves*, Van Nostrand Reinhold, New York, 1992.
9 M. M. J. Treacy, J. B. Higgins and R. von Ballmoos, *Collection of Simulated XRD Powder Patterns for Zeolite*, Elsevier, The Netherlands, 3rd edn., 1996.
10 P. Ganguly and T. Somsundaram, *Appl. Phys. Lett.*, 1980, **43**, 160.
11 T. Somsundaram and P. Ganguly, *J. Appl. Phys.*, 1985, **57**, 5043.
12 A. Rosencwaig and A. Gersho, *J. Appl. Phys.*, 1976, **47**, 64.
13 J. M. Bennett, J. M. Cohen, G. Artioli, J. J. Pluth and J. V. Smith, *Inorg. Chem.*, 1985, **24**, 188.
14 J. B. Parise and C. S. Day, *Acta Crystallogr., Sect. C: Cryst. Struct. Commun.*, 1985, **41**, 515.
15 J. M. Bennett, W. J. Dytrych, J. J. Pluth, J. W. Richardson Jr. and J. V. Smith, *Zeolite*, 1986, **6**, 349.
16 J. W. Richardson Jr., J. V. Smith and J. J. Pluth, *J. Phys. Chem.*, 1990, **94**, 3365.
17 R. Jeinek, B. F. Chmelka, Y. Wu, P. J. Grandinetti, A. Pines, J. Barrie and J. Klinowski, *J. Am. Chem. Soc.*, 1991, **113**, 4097.
18 W. M. Meier, D. H. Olson and Ch. Baerlocher, *Atlas of Zeolite Structure Types*, Elsevier, The Netherlands, 4th edn., 1996.
19 J. J. Pluth and J. V. Smith, *Nature (London)*, 1985, **318**, 165.
20 E. B. Keller, W. M. Meier and R. M. Kirchner, *Solid State Ionics*, 1990, **43**, 93

Paper 7/02997G; *Received* 1*st May*, 1997